First publ. in: Physical Review B 67 (2003), 155206

Inversionless amplification of coherent terahertz radiation

C. Janke,* P. Haring Bolivar, A. Bartels, and H. Kurz
Institut für Halbleitertechnik, RWTH Aachen, D-52056 Aachen, Germany

H. Künzel
Heinrich-Hertz-Institut für Nachrichtentechnik, D-10587 Berlin, Germany

We experimentally demonstrate inversionless amplification of the emission from electronic transitions in a solid state system inside a cavity. A semiconductor-based terahertz (THz) emitter is exposed to a coherent, phasematched THz background field during the emission process leading to an increase in the overall emitted THz power of more than one order of magnitude. The experimental concept and results are discussed within a three-level model and an extended density matrix approach.

Time-resolved spectroscopy and imaging in the THz region of the electromagnetic spectrum are important and growing fields of research with a wide range of applications.[1] Many of these applications are, however, hampered by the insufficient power and efficiency of the available THz sources. Up to now, a variety of broadband[2–4] and tunable[5,6] THz sources has been developed. Most of these sources rely on the coherent motion of charge carrier distributions created by impulsive excitation with femtosecond laser pulses, for example, the widely used semiconductor surface field emitter. In this type of emitter, the photogenerated carriers are accelerated by the semiconductor surface field and emit pulsed THz radiation.[7] The optical-to-THz conversion efficiency of such impulsively excited emitters is on the order of 10^{-5}. One of the main limitations to the efficiency is the fast loss of coherence due to carrier-carrier scattering. This restricts the coherent motion of the photoexcited charge carrier ensemble and the coherent emission time is limited to a small fraction of the intrinsic radiative lifetime,[5] typically below 10^{-3}. Consequently, only a small fraction of the energy deposited in the system is emitted coherently. The remaining part is dissipated in an incoherent manner and, thus, unusable for time-domain experiments. Considerable amount of interest is therefore directed towards possible ways of increasing THz emitter efficiency.

Here, we report an increase of the overall emitted THz power of more than one order of magnitude via amplification without inversion (AWI) (Refs. 8–10) for a semiconductor surface field emitter. By exposing the emitter to a coherent, phasematched THz background field during the emission process[11] more energy is radiated before coherence is lost and the amount of coherently emitted THz radiation is amplified. This concept is experimentally implemented by placing the emitter inside a high repetition rate THz resonator and synchronously optically exciting it with a femtosecond laser source. Our results constitute the first experimental demonstration of AWI on electronic transitions of a solid state system. Previously, AWI has only been observed on magnetic field coupled transitions in gases (e.g., Refs. 12,13) and for coherent atomic matter waves.[14,15] Related phenomena on Fano type interferences and electromagnetically induced transparency (EIT) were reported for certain quantum well structures by Faist *et al.*[16] and Schmidt *et al.*,[17] respectively. For a more general overview on the topic see, e.g., Scully and Zhu (Ref. 18 and references therein). Due to the inversionless nature of the amplification effect we believe our results to be of considerable fundamental and practical interest.

In order to demonstrate the generality of the adopted amplification mechanism we use a three-level model and a density matrix approach for our theoretical analysis. The three-level system (Fig. 1) serves as the minimal description of an impulsively excited THz emitter based on the coherent motion of charge carriers. It allows to model the photoexcitation from a ground level $|0\rangle$ to a superposition of electronic states $|1\rangle$ and $|2\rangle$ which oscillates in space and thereby emits THz radiation. The energy gap between the ground level $|0\rangle$ and levels $|1\rangle$ and $|2\rangle$ corresponds to optical frequencies, the upper two levels $|1\rangle$ and $|2\rangle$ are separated by a few meV corresponding to THz frequencies. More complex THz emitters can be described by taking more states into account, but this simple system already contains the basic characteristics of any charge motion related THz emitter. As real particle excitations and correlations are excited by the laser—which have complicated interaction pathways under the influence of

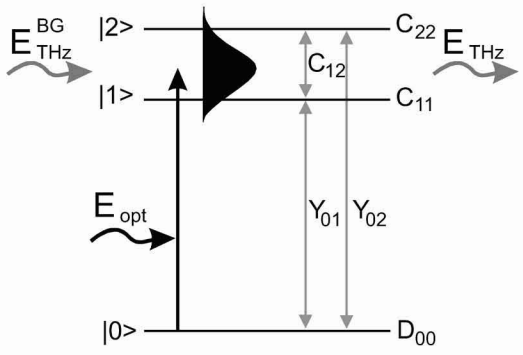

FIG. 1. Three-level model for an impulsively excited THz emitter. The upper two levels are responsible for the emission of THz radiation. The influence of a THz background field $E_{\mathrm{THz}}^{\mathrm{BG}}$ in addition to the exciting laser field E_{opt} is studied by use of a density matrix approach. C, D, and Y denote the intraband and interband population densities and polarizations, respectively.

the THz background field—a simpler description of the amplification mechanism via a parametric effect is problematic.

Generally, intraband and interband dynamics are adequately treated using a density matrix approach.[19] We adopt this approach and extend it as described in Ref. 20 to take the influence of a THz background field $E_{\mathrm{THz}}^{\mathrm{BG}}$ in addition to the exciting laser field E_{opt} into account. Six coupled equations are derived for the time evolution of the population densities of electrons C_{ii} and holes D_{00}, the intraband polarizations C_{ij} and for the optical interband polarizations Y_{0i}:

$$\frac{d}{dt}C_{ii} = -\frac{1}{T_1}C_{ii} + \frac{i}{\hbar}[\mu_{i0}E_0\hat{Y}_{0i}^* - \mu_{i0}^*E_0^*\hat{Y}_{0i}] + \frac{i}{\hbar}E_{\mathrm{THz}}^{\mathrm{BG}}[\mu_{ij}C_{ij} - \mu_{ji}C_{ji}],$$

$$\frac{d}{dt}C_{ij} = -\left[\frac{1}{T_{2,\mathrm{intra}}} + i\omega_{ij}\right]C_{ij} + \frac{i}{\hbar}[\mu_{j0}E_0\hat{Y}_{0i}^* - \mu_{i0}^*E_0^*\hat{Y}_{0j}] + \frac{i}{\hbar}E_{\mathrm{THz}}^{\mathrm{BG}}[\mu_{ji}C_{ii} - \mu_{ji}C_{jj}],$$

$$\frac{d}{dt}\hat{Y}_{0i} = -\left[\frac{1}{T_{2,\mathrm{inter}}} + i(\omega_{i0} - \omega_L)\right]\hat{Y}_{0i} + \frac{i}{\hbar}E_0[\mu_{i0} - \mu_{i0}C_{ii} - \mu_{j0}C_{ji} - \mu_{i0}D_{00}] - \frac{i}{\hbar}E_{\mathrm{THz}}^{\mathrm{BG}}\mu_{ij}\hat{Y}_{0j}$$

for $i,j=1,2$ and $D_{00}=C_{11}+C_{22}$. E_0 and ω_L are the amplitude and frequency of the exciting laser field, μ_{ij} the transition matrix elements and ω_{ij} the respective transition frequencies (where $\omega_{ij}=\omega_i-\omega_j$). T_1 and T_2 are phenomenological relaxation and dephasing times, where the energy relaxation time T_1 is typically long compared to the picosecond intraband and interband dephasing times T_2 and arbitrarily chosen to be 1 ns. A rotating wave approximation for the exciting laser field E_{opt} and the interband polarization Y_{0i} has been included in the above equations by setting $E_{\mathrm{opt}}(t)=E_0(t)\cdot e^{-i\omega_L t}+E_0^*(t)\cdot e^{+i\omega_L t}$ and $Y_{0i}(t)=\hat{Y}_{0i}(t)\cdot e^{-i\omega_L t}$. The population densities C_{11} and C_{22} of the upper two levels are numerically derived from the above equations and displayed in Fig. 2. The vertical dashed line indicates the dephasing time, i.e., the coherence time of the system which is taken to be 1 ps. Initially, both levels are equally populated by broadband optical excitation at $t=0$ with a 100 fs FWHM Gaussian shaped laser pulse. In absence of a THz background field [Fig. 2(a)] the population of both states remains equal, as reflected by the congruence of the curves for C_{11} and C_{22}, while slowly decaying to the ground state by energy relaxation. In contrast, an additional, resonant THz background field can be employed to drive a population change, evident by the splitting of the curves in Figs. 2(b)–2(d). For clarity, a single-cycle THz background field of large magnitude centered at 1 THz is assumed in the calculation. The sooner the THz background field is present after the optical excitation, the less coherence has been lost by dephasing and the larger the population change will be as shown in Figs. 2(b) and 2(c) for two different arrival times of

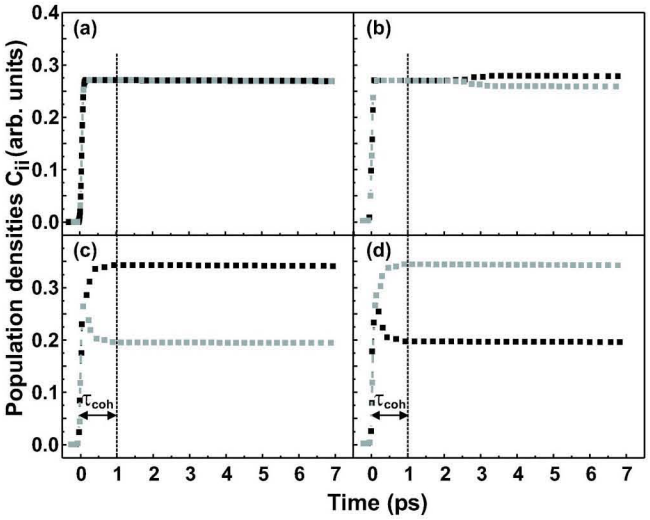

FIG. 2. Density matrix calculation. Shown are the population densities of the upper two levels of the three-level system C_{11} (black squares) and C_{22} (gray squares) as a function of time for (a) no additional THz background (BG) field, (b) additional THz BG field present 2 ps after optical excitation, (c) THz BG field present 50 fs after optical excitation, and (d) THz BG field with inverted phase with respect to (c). The vertical dashed line indicates the coherence time of 1 ps.

2 ps and 50 fs. In both cases, the population of the lower level C_{11} is increased while that of the upper level C_{22} is decreased which signifies emission. For a THz background field with inverted phase [Fig. 2(d)] the effect is reversed, i.e., the population of the lower level C_{11} is decreased while that of the upper level C_{22} is increased which signifies absorption. Since this type of emission or absorption is an additional effect induced by the THz background field, the emitted THz power can be amplified as well as attenuated. The phase dependence is a direct consequence of the fact that the inversionless amplification effect is based on the interaction of the THz background field with the coherent polarization between levels $|1\rangle$ and $|2\rangle$. It is thus mandatory to externally control the phase of the THz background field to accomplish amplification. At large, if a THz background field is present as long as coherence prevails in the system and the phase is set accordingly, emission will be amplified without the need for population inversion. Furthermore, the larger the magnitude of the THz background field is and the less coherence has been lost by dephasing, the larger the gain will be. Ideally, the total energy deposited in the system is emitted before dephasing sets in. This would yield a maximum possible gain of about three orders of magnitude.

Experimentally, the amplification of coherent THz radiation is realized by use of a specific THz resonator, as sketched in Fig. 3. The pulse train from a 1 GHz repetition-rate Ti:sapphire femtosecond laser source[21] is split into excitation and probe pulses. First, pulsed THz radiation is generated and detected in a standard configuration [Fig. 3(a)] using bulk InGaAs as surface field emitter, two off-axis paraboloids and a photoconductive antenna as receiver in a typical time-domain THz emission setup. This standard configuration is used to quantify the THz emission in absence of

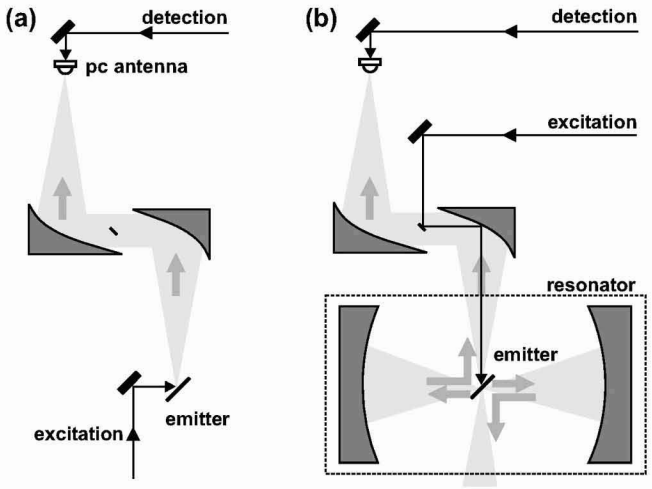

FIG. 3. Experimental setup. (a) Standard configuration to generate and detect THz radiation with an InGaAs surface field emitter and a photoconductive (pc) antenna as receiver in a typical time-domain THz emission setup. The THz beam path is indicated by the area colored in light gray. (b) THz resonator setup with modified excitation path. Two spherical mirrors comprise the THz resonator.

a THz background field. The THz resonator is then formed by surrounding the emitter with two spherical mirrors, as shown in Fig. 3(b). The direction of excitation is changed so that the THz pulses generated in the specular reflection direction will travel back and forth between the resonator mirrors and provide the THz background field for the emitter. With this reverse excitation scheme the effect of the resonator can be evaluated by direct comparison as the detection path remains unchanged in both configurations. Inside the THz resonator most of the impinging radiation is transmitted through the emitter, the residual reflectivity is exploited by using the emitter itself as output coupler. Due to the linear geometry of the resonator, half of the available radiation is coupled out into the direction opposite to the detection path and, thus, lost for the experiment.

To ensure optical pumping of the emitter synchronous to the impinging THz background field, the cavity lengths L (repetition rates f_{rep}, respectively) of the exciting laser and THz resonator must be identical. The 1 GHz repetition rate of the exciting laser allows to build a compact THz resonator with a round trip length of only 30 cm ($f_{\mathrm{rep}}=c/L$, where c is the speed of light). This gives clear advantages with respect to alignment and handling compared to previous attempts with a conventional 80 MHz system which required a roundtrip length of roughly four meters.[11] To ensure that the THz background field has the correct phase relationship in order to achieve amplification, the overall roundtrip phase change has to be a multiple of 2π. Here the Gouy effect, which introduces an extra phase shift of π for each focus passed through, has to be taken into account. This requires the resonator geometry to be near concentric. Furthermore, it is crucial to control and minimize the resonator loss; the loss introduced by the resonator mirrors is negligible compared to that stemming from the emitter. The latter is considerably reduced by thinning the emitter and by applying an antireflection coating.

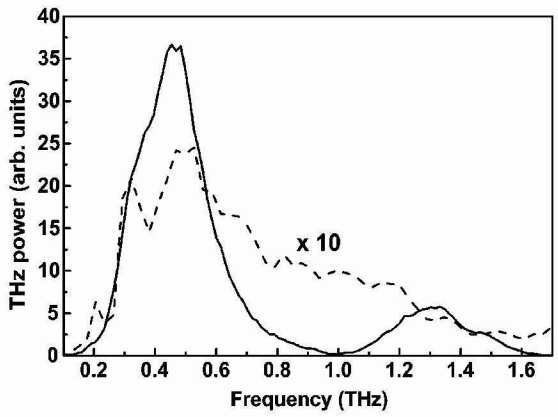

FIG. 4. Spectral intensity of amplified emission (solid line) and standard emission (dashed line) of the same emitter on a linear scale. The latter is magnified by a factor of 10 for clarity.

Time-resolved experiments are performed with the standard emission setup and in the THz resonator configuration for the same emitter. For evaluation purposes the time-domain measurement data is converted into frequency space by Fourier transformation. The amplification effect can then be determined by straightforward comparison. The main result is shown on a linear scale in Fig. 4. The spectral intensity of the THz emission is amplified by roughly a factor of 15 for frequencies between 0.3 and 0.6 THz (solid line) compared to the spectral intensity of the same emitter without resonator (dashed line, magnified by a factor of 10 for clarity). Over the integral of the spectrum the gain amounts to more than one order of magnitude. We estimate the total emitted power in this case to be on the order of 10 μW. In the light of losing half of the available radiation due to the adverse outcoupling effect mentioned above, this result emphasizes the potential of our concept. The dip at 1 THz is caused by the transmission characteristics of the emitter, modulating both the intracavity transmission as well as the output coupling from the THz resonator. Because transmission through the emitter is close to unity around 1 THz, these frequency components are trapped inside the resonator. Thus, by further optimizing the emitter with respect to its transmission characteristics and outcoupling ratio, still higher gain is feasible.

To experimentally demonstrate the phase dependency observed in the density matrix calculation, additional measurements were performed with a slightly detuned resonator. The detuning leads to erroneous synchronization of the optical pumping of the emitter and the impinging THz background field in the time domain. The temporally short THz pulse providing the background field for the emitter consists of a superposition of individual frequency components with a certain phase relationship. Therefore, a temporal detuning Δt corresponds to a linear phase shift $\Delta\varphi(\nu)=2\pi\nu\Delta t$ for a certain frequency component ν of the THz background field. The resulting running phase thus allows us to test the phase dependence of the THz background field while avoiding modifications to the resonator geometry. This allows us to work under identical experimental conditions with respect to the synchronized case. The result is shown in Fig. 5 on a

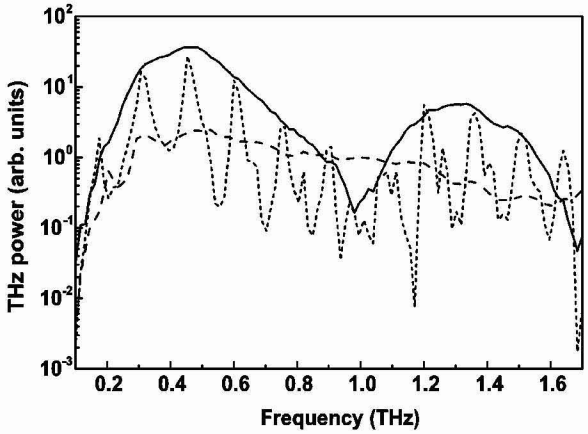

FIG. 5. Spectral intensity of amplified emission (solid line), standard emission (dashed line), and for a slightly detuned resonator (dotted line) on a logarithmic scale.

logarithmic scale (dotted line). Also shown are amplified emission (solid line) and standard emission (dashed line). In the detuned case, the spectrum is strongly modulated with the modulation swing centered on the standard emission and the amplified emission as maximum. The modulation period corresponds to the inverse of the temporal detuning. Evidently, only some frequency components are in fact amplified [where $\Delta\varphi(\nu)=2\pi n, n=0,1,2,\ldots$] while others are attenuated, each by roughly the same factor (dotted line above or below dashed line). Thus, amplification as well as attenuation can be achieved depending on the relative phase of the THz background field. This is a clear indication of the inversionless nature of the amplification effect.

In summary, by placing a surface-field THz emitter inside a cavity net amplification of the emitted THz power is achieved. This constitutes experimental observation of AWI in a solid state system. The gain amounts to more than one order of magnitude. The results indicate that by adjusting the delicate balance between intracavity losses and output coupling ratio more precisely, further enhancements are feasible. In addition, the presented concept is not limited to the specific type of THz emitter used, but should be applicable to other types of charge carrier related emitter systems.

We thank A. Stahl and R. Martini for valuable discussions and acknowledge the financial support of the *Deutsche Forschungsgemeinschaft*.

*Electronic address: janke@iht rwth-aachen.de

[1] M. Nuss and J. Orenstein, *Millimeter and Sub-Millimeter Waves*, edited by G. Gruener (Springer Verlag, Heidelberg, 1998).

[2] P. Smith, D. Auston, and M. Nuss, IEEE J. Quantum Electron. **QE-24**, 255 (1988).

[3] C. Fattinger and D. Grischkowsky, Appl. Phys. Lett. **54**, 490 (1989).

[4] X.-C. Zhang, B. Hu, J. Darrow, and D. Auston, Appl. Phys. Lett. **55**, 337 (1990).

[5] H. Roskos, M. Nuss, J. Shah, K. Leo, and D. Miller, Phys. Rev. Lett. **68**, 2216 (1992).

[6] C. Waschke, H. Roskos, R. Schwedler, K. Leo, H. Kurz, and K. Köhler, Phys. Rev. Lett. **70**, 3319 (1993).

[7] X.-C. Zhang and D. Auston, J. Appl. Phys. **71**, 326 (1992).

[8] O. Kocharovskaya, Phys. Rep. **219**, 175 (1992).

[9] C. Keitel, O. Kocharovskaya, L. Narducci, M. Scully, and S.-Y. Zhu, Phys. Rev. A **48**, 3196 (1993).

[10] A. Belyanin, C. Bentley, F. Capasso, O. Kocharovskaya, and M. Scully, Phys. Rev. A **64**, 013814 (2001).

[11] R. Martini, F. Hilbk-Kortenbruck, P. Haring Bolivar, and H. Kurz, in *6th International Conference on THz Electronics Proceedings THz 98* (IEEE, New York, 1998), p. 242.

[12] A. Nottelmann, C. Peters, and W. Lange, Phys. Rev. Lett. **70**, 1783 (1993).

[13] W. van der Veer, R. van Diest, A. Dönzelmann, and H. van Linden van den Heuvell, Phys. Rev. Lett. **70**, 3243 (1993).

[14] M. Kozuma, Y. Suzuki, Y. Torii, T. Suguira, T. Kuga, E. Hagley, and L. Deng, Science **286**, 2309 (1999).

[15] S. Inouye, T. Pfau, S. Gupta, A. Chikkatur, A. Görlitz, D. Pritchard, and W. Ketterle, Nature (London) **402**, 641 (1999).

[16] J. Faist, F. Capasso, C. Sirtori, K. West, and L. Pfeiffer, Nature (London) **390**, 589 (1997).

[17] H. Schmidt, K. Campman, A. Gossard, and A. Imamoglu, Appl. Phys. Lett. **70**, 3455 (1997).

[18] M. Scully and S.-Y. Zhu, Science **281**, 1973 (1998).

[19] M. Luo, S. Chuang, P. Planken, I. Brener, H. Roskos, and M. Nuss, IEEE J. Quantum Electron. **QE-30**, 1478 (1994).

[20] T. Kuhn, *Theory of Transport Properties of Semiconductor Nanostructures*, edited by E. Schoell (Chapman and Hall, London, 1998).

[21] A. Bartels, T. Dekorsy, and H. Kurz, Opt. Lett. **24**, 996 (1999).